FINDING SHIP PROPELLER PROFILES WITH THE LEAST CRITICAL CAVITATION NUMBER

É. L. Amromin, A. V. Vasil'ev, and E. Ya. Semionicheva

UDC 532.5:621.22

Undesired consequences in the beginning stages of blade cavitation often limit allowable propeller speeds, which usually are characterized by the critical cavitation number. These speeds can be increased by choosing the proper profiles of the cylindrical sections of the propeller. The principle of such a choice has been given [1] for the plane uniform stationary flow of an ideal fluid. According to this principle, the smallest cavitation number is attained by the profile of a set with identical lift coefficients, which has the largest minimum pressure along the isobaric section on the lift side. Specific examples of such blade profiles have constructed [2, 3]. However, practical use of optimum [1-3] profiles for cylindrical sections of propeller blades on test stands [4] has led to ambiguous results: while water tunnel tests of model propellers designed from [1] give a measured critical cavitation number σ_i, which is much less than the value of σ_i for prototype propellers, actual ship propellers of the same shape exhibit both smaller and significantly higher values of σ_i.

In order to understand this situation, which arises in attempts to apply the theory [1] in engineering practice, the assumptions of this theory must be analyzed for flow conditions around blades. In view of the complexity of such calculations under natural conditions, we analyze a series of model problems to evaluate the assumptions. In the first problem, we examine the consequences of the widely used engineering technique of separately finding the thickness and curvature of the flat sections of the blades. In the second, we combine the results of the theory [1], which assumes that the cavity dimensions are infinitely small, and more accurate computations of the critical cavitation number, which include finite cavity dimensions. In the third problem we investigate how the nonuniformity of the flow against the blade in the boundary layer of the ship's hull affects the pressure distribution and the conditions for creating cavitation on the blade profiles.

1. The assumptions and results used [4] in the theory [1-3] are related to a plane uniform incoming flow, while the highly three-dimensional flow around the blades makes the flow at each cylindrical cross section nonuniform and variable along the chord. To some degree, this nonuniformity is considered by a widely used technique [5] of separately specifying the thickness and curvature of the profile midline: the stationary nonuniformity is considered approximately by the change of curvature in the cross section profile as compared to the solution to the plane problem. The primary basis of this change is the same as for the change in the angles of attack of blade cross sections in going from one section to another. Then the thickness should be found from the reverse solution of blade theory, by a formal comparison with the problem of the ideal cavitation profile [6]:

$$\Delta\Phi = 0; \tag{1.1}$$

$$\partial\Phi/\partial N|_S = 0; \tag{1.2}$$

$$\lim_{x^2+y^2\to\infty}\left(1+\frac{x+y\,\mathrm{tg}\,\alpha}{\Phi}\right)=0; \tag{1.3}$$

$$\frac{\partial\Phi}{\partial T}\{1, 0\} = 0; \tag{1.4}$$

$$\left.\frac{\partial\Phi}{\partial T}\right|_{S_k} = \gamma_0; \tag{1.5}$$

Leningrad. Translated from Zhurnal Prikladnoi Mekhaniki i Tekhnicheskoi Fiziki, No. 5, pp. 47-52, September-October, 1991. Original article submitted May 3, 1990.

 0021-8944/91/3205-0692$12.50

$$N_y(x_2) = N_0; \tag{1.6}$$

$$2\oint\limits_{(S)} \frac{\partial \Phi}{\partial T} dS = C_y^*. \tag{1.7}$$

Here S is the total surface of the profile; S_k is an isobaric section of S; T and N are the tangent and normal unit vectors to S; α is the angle of attack; {x, y} = {1, 0} are the coordinates of the aft sharp edge of the profile at which the Zhukovskii–Chaplygin condition (1.4) is satisfied; C_y^* is a given value of C_y; and x_2 is the abscissa of the point at which S_k is connected to the tail section of the profile S_f. The constant γ_0 is chosen such that (1.6) is satisfied; that is, the continuity of the normal to S is maintained. The shape of the leading side of the profile over the whole range of values of the lift coefficients $C_y^{**} < C_y < C_y^*$ must satisfy the condition $C_{pm} = \gamma_0^2 - 1$ for $C_{pm} = |\min C_p|$, where C_p is the dimensionless pressure coefficient. For symmetric profiles, $C_y^{**} = -C_y^*$ and the beginning of S_k should be set [2] at the forward edge {x, y} = {0, 0}. The simplest choice for S_f is a wedge with a given acute angle θ of the trailing edge. The profile shape is sought by roughly the same sequence of operations used for solving the nonlinear ideal cavitation problem [6].

Typical shapes of the profile thickness, which are constructed in this manner are shown in Fig. 1, where the numbers on the curves are the corresponding values of C_y^* and C is the chord of the profile. The dependence of C_{pm} on the largest thickness δ of this family of profiles, shown on the left part of Fig. 2, determines the smallest values of C_{pm}, which in principle can be attained on symmetric blade profiles for given values of C_y^* (the values shown near the calculated curves) and a given type of S_f. These values are weakly dependent on the shape of S_f: curves on the left part of Fig. 2 correspond to profiles with wedge-shaped S_f's, but the black dots correspond to profiles with parabolic S_f's, and they practically lie on the curves, even for relatively long S_f's, which correspond to small C_y^*'s. Therefore these functions can be considered universal for symmetric profiles which are optimum in the sense of [1]. The center section of Fig. 2 compares curves of $C_{pm}(C_y)$ for these profiles (the solid curves 1 and 2) and for profiles that are known to have high properties from NACA-0012 and NACA-66 with the same δ (dashed curves 1 and 2). These data confirm the assertion that values of C_{pm} no higher than for a given profile of the type in NACA-66 are provided in a narrower range of attack angles or C_y values.

Because the extension of the blade is on the order of unity, changes in the profile curvature, using the techniques in [5], can be rather large (for example on the order of 0.02). If the selection of partitions were optimum in this case, then the constructed symmetric profiles could be treated as optimum in the sense [1] of the optimum thickness distribution; but solid curve 3 in the central part of Fig. 2 shows that the combination of the same thickness as in curve 2 with the NACA curvature a = 0.8 is worse than the curve for the NACA-66 diagram with the same δ and the largest relative curvature $\delta_c = 0.02$ (the dashed curve 3). These results demonstrate that the separation of the profile shape into curvature and thickness is not optimum and can have an excessive C_{pm}.

2. However, C_{pm} cannot be set equal to σ_i; they are equal only for infinitely small cavities. Actually, because of surface-tension forces, the dimensions of the cavity and radius of curvature of its boundary r can not be set to be too small. The equilibrium condition of this boundary is expressed by Laplace's formula

$$p_K = p + 2\tilde{\gamma} r^{-1}, \tag{2.1}$$

where $\tilde{\gamma}$ is the surface tension coefficient on the boundary between the gas and the liquid; and p_K and p are the pressures on opposite sides of the boundary. The wettability of the blade surface requires a large curvature of this boundary near the line where the boundary joints the streamlined body. The minimum cavity dimensions which satisfy (2.1) are negligibly small compared to the blade extension; however, these values of r are the same order of

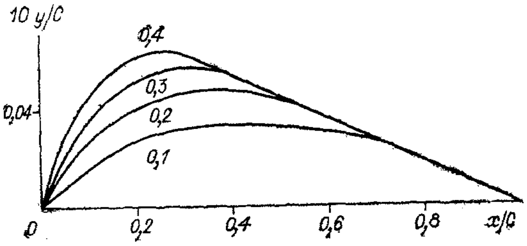

Fig. 1

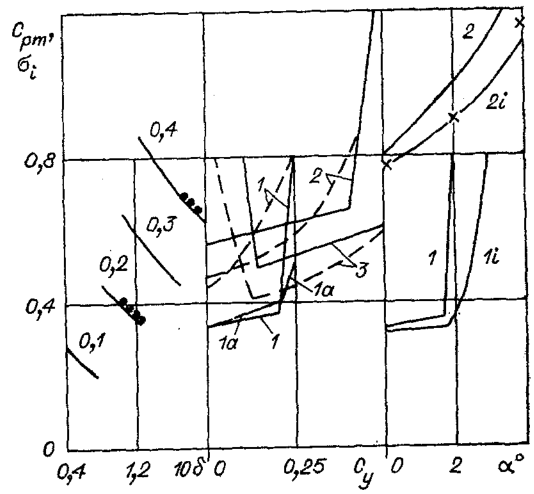

Fig. 2

magnitude as the boundary layer thickness of the profile near the leading edge. Therefore the cavity causes a local pressure redistribution, similar to an obstacle in the boundary layer. The fundamentals of the theory, the method, and a calculated example of the initial stages of cavitation are given in [7] and [8]. Here the right side of Fig. 2 only shows how C_{pm} and σ_i can differ: curve 2i is the calculated function σ_i (α) for the profile NACA-4412 for Re = $2 \cdot 10^6$ and C = 0.1 m; curve 2 shows $C_{pm}(\alpha)$ for this profile; × shows experimental values of $\sigma_i(\alpha)$ taken from [9]. The correlation is excellent. Curves 1i and 1 are the functions $\sigma_i(\alpha)$ and $C_{pm}(\alpha)$ for the optimum (per [1]) 12% profile already shown in Fig. 2. Curve 1i corresponds to the same Re, C, and δ used for 2i. The depression of σ_i, compared to C_{pm}, is roughly the same for both traditional and optimum [1] profiles. Therefore, the reported [4] disagreement between theory [1-3] and experiment cannot explain the significantly different effect of viscosity and capillary attraction on the different profiles.

3. However, the profiles obtained here and in [2] and [3] were constructed for a stationary incident flow, while the blades of hydraulic machinery usually intersect a nonuniform flow as they turn, because the flow around them is not stationary, even for a constant blade rotation rate. In order to avoid overestimating the effect of the nonuniformity, this variability must be considered in the estimates. The effect of nonstationary incident flow around blade profiles usually is analyzed theoretically within the framework of a mechanically ideal fluid [10, 11]. If this nonuniformity is modeled with the use of a combination of hydrodynamic singularities which are adjusted relative to the profile, then the flow remains as a potential flow, and the curve for Φ, along with (1.1)-(1.4), will conserve vorticity

$$\oint_{(S)} \frac{\partial \Phi}{\partial T} dS - \sum_i \Gamma_i = \text{const}, \tag{3.1}$$

where Γ_i is the intensity of the vortices in the flow. These calculations use a simplifying assumption on the vortex sheet behind the profile: it deviates negligibly from the established curve. The correspondence of rsults of such calculations with experiments can be judged from Fig. 3, in which calculated and measured [12] pulsation amplitudes of the dimensionless pressure coefficient C_p' on the lift side of the blade are compared with the NACA-0012 profile. The instability of the flow in these tests was created by a rotating elliptical

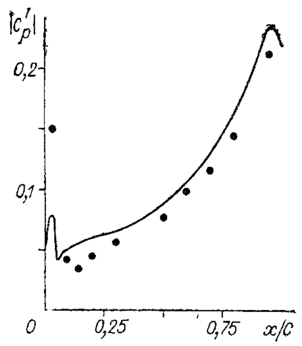

Fig. 3

cylinder. The resultant pulsations in the absence of the blade were measured and presented in [12]. It proved possible to represent Φ in (1.1)-(1.4) and (3.1) in the form

$$\Phi = \Phi_1 + \Phi_2 + \Phi_3 - x - y \operatorname{tg} \alpha, \tag{3.2}$$

where Φ_1 is the potential for perturbations from the rotating cylinder, which is approximated as the sum of potentials for singularities of constant and variable intensity, which are selected from measurements of the flow velocity in the tunnel at the location of the blade in its absence; Φ_2 is the potential of the vortex sheet, which depends only on one unknown — the intensity of the time-dependent vortex from the trailing edge; Φ_3 is the potential of distributed singularities in the limits of the profile, whose intensity values can be deterined from (1.1)-(1.4) and (3.1) for any t. As far as can be judged from Fig. 3, the calculated pulsations are barely higher than the experimental ones; therefore the calculated surges of C_{pm} in a nonuniform nonstationary flow evidently will not exceed the experimental surges.

The nonuniformity, which is characteristic for the incident flow around a propeller blade [5] and which is caused by the nonuniformity of the velocity field in the boundary layer of the ship's hull, can also be modeled conveniently with the assumption (3.2). In the results of such calculations presented below, Φ_1 is the potential of a source—sink pair drifting past the profile. The distance between the singularities and their intensity were varied in a way to guarantee a given width λ of the zone of nonuniformity, within which $V = -\partial\Phi_1/\partial y$ drops an order of magnitude from a given value V_m.

Figure 4 shows the dependence of C_{pm} and C_y on the dimensionless time $\tau = tU_\infty/C$ for various profiles and potentials Φ_1. These curves were calculated by solving (1.1)-(1.4) and (3.1). In all cases, $\tau = 0$ ($\tau = 1$) corresponds to the leading (trailing) edge passing through the average of the nonuniformity. Curves 1 and 2 are the functions $C_y(\tau)$ of the NACA-0012 profile with $\delta = 0.12$ for $\alpha = \pi/180$ and $\pi/90$, respectively, for $\lambda = 0.5$ C and $V_m = \pi/90$. The points which are practically identical to curve 2 (on the scale of Fig. 4) are the function $C_y(\tau)$ for the optimum (per [1]) 12% profile in a flow with the same nonuniformity. The curves 1c and 2c are for the NACA-0012 profile and correspond to the function $C_{pm}(\tau)$ for the same conditions as for curves 1 and 2. Curves 1b and 2b are the analogous functions for the optimum profile. In analyzing the functions in Fig. 4, we note the absence of a mutually identical correspondence of C_{pm} and C_y. We also note not only the strong dependence of surges in C_{pm} on the profile shape, but also the significant phase shift between $C_y(\tau)$ and $C_{pm}(\tau)$. The surge in C_{pm} when the leading edge passes through the nonuniformity increases with $\partial C_{pm}/\partial C_y$, and the optimum (per [1]) profile has a significant advantage only when the uniformity excites a state relative to the center "platform" of the diagram of $C_{pm}(C_y)$, and not to its side branches. Here, as can be seen from a comparison of the curves in Figs. 2 and 4, the local growth in $|\partial\Phi/\partial y|$ in a nonuniformity with $\lambda \lesssim C$ not only does not determine the surges in C_{pm}, but it is doubtful that C_{pm} can be found from the results for a stationary uniform flow.

The possibilities of quasistationary calculations for nonuniform flows are illustrated in Fig. 5, which shows the results for the NACA-0012 profile for the same $V_m = \pi/90$. Here curve 1 is the function $C_y(\tau)$ for $\alpha = 0$ and $\lambda = C/2$; curve 2 is for $\alpha = 0$ and $\lambda = C/2$; curve 2 is for $\alpha = 0$ and $\lambda = 3C$; and curve 3 is for $\alpha = \pi/90$ and $\lambda = C/2$. The solid curves are

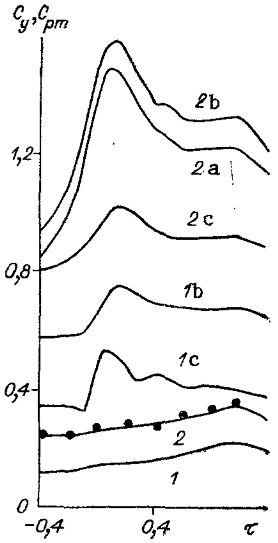

Fig. 4

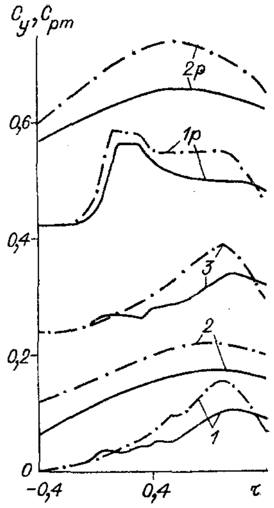

Fig. 5

for the nonstationary theory. The dashed curves are for the quasistationary theory in which $\Phi_2 = 0$ and (3.1) is not used, but $\Phi_1(\tau)$ is the same. Curves 1p and 2p are the functions C_{pm} for the same conditions as curves 1 and 2. The quasistationary approach leads to a quantitative difference from the nonstationary theory, but nonetheless there is no significant phase shift between them. In both cases surges in C_{pm} become stronger as λ and δ^{-1} increase for constant V_m. There can be no incident flow, because the time to pass through the nonuniformity is $\tau \geq 0.01$ sec; that is, sufficient to form a cavity.

In conclusion, the model problem shows that the lack of success [4] in applying the theory [1] to propellers is most likely due to the nonuniformity of the incident flow on the blade. So far as can be judged from curve 2a (Fig. 4), some advantage in C_{pm} can be reached by rounding the leading edge — with a corresponding decrease of the isobaric section in solving (1.1)-(1.7). Then curve 2a corresponds to the same flow as 2b, and the function $C_{pm}(C_y)$ is given by curve 1a in the central part of Fig. 2 for the uniform incident flow for the same profile. The fundamental possibility of formulating this problem for a computer program is also obvious. However, the relatively small phase shift of the identical dot-dash and solid curves in Fig. 5 show that one can hope for the existence of a small set of characteristic quasistationary reverse problems for nonuniform flows, which makes it possible to optimize the nonstationary flow profiles. Evidently, the basic difficulty now is to formulate these problems.

The authors are indebted to A. N. Ivanov for useful discussions.

LITERATURE CITED

1. P. R. Garabedian and D. C. Spencer, "Extremal methods in cavitation flow," J. Rational Mech. Anal., No. 1 (1952).
2. R. Eppler and T. Shen, "Wing section for hydrofoils," J. Ship Res., No. 3 (1979).
3. K. V. Aleksandrova, "Calculation and design of cavitation profiles," Tr. NTO SP (Trans. Scientific and Technical Society of the Shipbuilding Industry), No. 332 (1980).
4. F. Peterson, Design, application, and test of propellers with new blade sections," 18th ITTC, London (1985).
5. Handbook on the Theory of Naval Architecture [in Russian], Vol. 1, Sudostroenie, Leningrad (1985).
6. A. N. Ivanov, Hydrodynamics of Developed Cavitation Flows [in Russian], Sudostroenie, Leningrad (1980).
7. É. L. Amromin, K. V. Aleksandrov, and Yu. L. Levkovskii, "Determining conditions for creating cavitation around bodies for flows with a discontinuity and an attachment of the boundary layer," Zh. Prikl. Mekh. Tekh. Fiz., No. 2 (1986).
8. É. L. Amromin, A. V. Vasil'ev, and V. V. Droblenkov, "Various approximations in the theory of cavitation flows of a viscous capillary fluid," Zh. Prikl. Mekh. Tekh. Fiz., No. 6 (1988).

9. J. H. J. van Meulen, "Boundary layer and cavitation studies of NACA-16012 and NACA-4412 hydrofoils," 13th Symposium on Naval Hydrodynamics, Tokyo (1980).
10. H. Attassi and M. E. Goldstein, "Unsteady aerodynamic forces acting on loaded two-dimensional blades in nonuniform incompressible flows," Symposium IUTAM sur l'Aeroelasticite dans les turbomachines, Paris (1976).
11. V. B. Kurzin and V. A. Yudin, "Calculation of the hydrodynamic interaction of a family of profiles with a consideration of the evolution of vortex trails," in: Modern Problems of Mechanics of Fluid and Gas [in Russian], Irkutsk (1988).
12. F. Lorber and E. E. Covert, "Unsteady airfoil pressures produced by periodic aerodynamic interference," AIAA J., No. 9 (1982).

NONSTATIONARY FLOWS OF AN INCOMPRESSIBLE VISCOUS FLUID WITH MEMORY IN CYLINDRICAL TUBES

A. D. Khon'kin UDC 533.6.011

In aerohydromechanical problems, the motion of a viscous thermally conducting gas traditionally is studied with the use of the Navier–Stokes equations, which are the result of the phenomenological closure of the conservation laws on the basis of linear transfer relations connecting the flow of momentum and energy with the spatial gradients of velocity and temperature – that is the transfer laws of Navier–Stokes and Fourier. In the case of slow quasistationary processes, these laws are derived from the kinetic Boltzmann equation with the use of the Chapman–Enskog method [1]. However, it has been shown [2, 3] that in the case of rapid nonstationary motions of a viscous thermally conducting gas, the expressions for the momentum and energy flows should include not only terms with spatial gradients of the velocity and temperature, but also time derivatives (accelerations) of these variables, which characterize the effects of temporal memory. The generalized hdyrodynamic equations [2, 3], which are called hydrodynamic equations for rapid processes, have been used to investigate the distribution of small perturbations, the structure of shock waves, diffusion, etc., and have been used to obtain a series of important results.

In this article, these hydrodynamic equations of rapid processes are used to study the nonstationary motions of a viscous incompressible fluid in circular cylindrical tubes. Exact solutions are found and analyzed for 1) the pulsating motion of the fluid due to a harmonically varying pressure gradient and 2) an instantaneously induced motion of an initially quiescent fluid.

1. For continuous media, the most general form of the laws of conservation of mass, momentum, and energy are written as

$$\frac{\partial\rho}{\partial t}+\frac{\partial\rho u_k}{\partial x_k}=0,\quad \rho\frac{\partial u_i}{\partial t}+\rho u_k\frac{\partial u_i}{\partial x_k}=-\frac{\partial p}{\partial x_i}-\frac{\partial P_{ik}}{\partial x_k},$$
$$\rho\frac{\partial e}{\partial t}+\rho u_k\frac{\partial e}{\partial x_k}=-p\frac{\partial u_k}{\partial x_k}-P_{ik}\frac{\partial u_i}{\partial x_k}-\frac{\partial Q_k}{\partial x_k}, \tag{1.1}$$

where ρ is the density; u_i ($i = 1, 2, 3$) are the velocity components along the x_i axis of the Cartesian coordinate system (x_1, x_2, x_3); p is the pressure, e is the internal energy; P_{ik} is the momentum flux (stress tensor); and Q_i is the thermal flux (energy flux). In order to obtain a closed system of equations from the conservation laws (1.1), the momentum and energy fluxes must be expressed in terms of parameters of the hydrodynamic state ρ, u_i, and e.

Zhukovskii. Translated from Zhurnal Prikladnoi Mekhaniki i Tekhnicheskoi Fiziki, No. 5, pp. 52-57, September-October, 1991. Original article submitted May 30, 1990.

0021-8944/91/3205-0697$12.50